Available online at www.sciencedirect.com
ScienceDirect
Thermochimica Acta 464 (2007) 7–15
thermochimica acta
www.elsevier.com/locate/tca

# Dehydration of a layered double hydroxide—$C_2AH_8$

N. Ukrainczyk [a,*], T. Matusinovic [a], S. Kurajica [a], B. Zimmermann [b], J. Sipusic [a]

[a] *Department for Inorganic Chemical Technology and Non-Metals, Faculty of Chemical Engineering and Technology, University of Zagreb, HR 10 000 Zagreb, Croatia*
[b] *Laboratory for Molecular Spectroscopy, Ruđer Bošković Institute, HR 10 000 Zagreb, Croatia*

Received 15 March 2007; received in revised form 5 July 2007; accepted 23 July 2007
Available online 15 August 2007

**Abstract**

Thermal dehydration of dicalcium aluminate hydrate, $C_2AH_8$, has been investigated by simultaneous differential thermal and thermo gravimetric analysis (DTA/TGA), powder X-ray diffraction (XRD), temperature-dependent infrared spectroscopy (FT-IR), and BET method of surface area measurement. The temperature-dependent infrared measurements were studied by two-dimensional infrared (2D-IR) correlation spectroscopy. The structure of aluminum-oxide polyhedron, characterized by $^{27}$Al solid state NMR spectrum method and FT-IR, shows tetrahedron and octahedron as the main forms of aluminum-oxide polyhedrons in $C_2AH_8$ sample. From the results obtained a variety of structural transformations observed are explained as a consequence of the removal of loosely held interlayer water molecules at lower temperatures, followed by grafting process of the interlayer $[Al(OH)_4]^-$ anion. Structural model of a grafting process of the interlayer $[Al(OH)_4]^-$ tetrahedron onto hydroxylated octahedrons of $[Ca_2Al(OH)_6]^+$ layers has been proposed in order to explain observed loss of one water molecule, shrinkage of interlayer spacing and qualitative changes of FT-IR spectra. At higher temperatures the dehydroxylation of the lattice and decomposition of the interlayer species occurs, yielding amorphous material that crystallizes into $C_3A$ and $C_{12}A_7$ at 885 °C. Those findings provide improvement in the interpretation of thermo-analytical results of calcium aluminate cements (CAC) hydration products, and better understanding of CAC conversion process.


*Keywords:* Calcium aluminate cement; $C_2AH_8$; Thermal decomposition; Dehydration; Layered double hydroxide; Grafting

## 1. Introduction

Although the hydration process of calcium aluminate cement (CAC) represents a process of commercial and industrial importance, the chemical processes involved during its hydration are not well understood yet [1–6]. The hydration of CAC is temperature dependent, yielding $CAH_{10}$ (cement notation: C(CaO), A($Al_2O_3$), H($H_2O$), c($CO_2$)) as main products at temperatures less than 10 °C, $C_2AH_8$ and $AH_3$ at about 30 °C and $C_3AH_6$ and $AH_3$ at temperatures greater than 55 °C. $CAH_{10}$ and $C_2AH_8$ are known to be metastable at ambient temperature and convert to the more stable $C_3AH_6$ and $AH_3$ with consequent material porosity increase and loss of strength. The conversion is accelerated by temperature and moisture availability for the dissolution and re-precipitation processes to take place [2]. On the other hand, in the absence of sufficient water, these phases do not convert but dehydrate. Due to a poor crystallinity of the hydration products formed at early age hydration and low water to cement ratio, the methods of combined thermal analysis (DTA/TGA) are promising ones regarding their qualitative and quantitative characterization. Previous works [6–19] indicated various interpretations of the results of thermal analysis of CAC hydration products, as shown summarized in Table 1. This can be primarily attributed to a vague understanding of the $C_2AH_8$ dehydration process. Structural and thermal decomposition studies of $CAH_{10}$, $C_2AH_8$ and $C_3AH_6$ [16,17,20–27] were undertaken in order to resolve structural transformations of calcium aluminate hydrate phases in temperature range 20–800 °C which considerably modify the thermomechanical behaviour of the material [6,17,18,28].

The aim of this work was to contribute to the better understanding of $C_2AH_8$ dehydration process during thermal analysis of CAC hydration products. In order to obtain detail information of the thermal evolution and structure of $C_2AH_8$ various measurement techniques were used. Beside commonly used techniques such as powder X-ray diffraction (XRD) and simul-

* Corresponding author.
*E-mail address:* nukrainc@fkit.hr (N. Ukrainczyk).

0040-6031/$ – see front matter © 2007 Elsevier B.V. All rights reserved.
doi:10.1016/j.tca.2007.07.022

Table 1
Decomposition temperatures of CAC hydration products in °C according to various studies, obtained by thermal analysis methods

| Reference | Year | Method | $CAH_{10}$ | $C_2AH_8$ | $C_3AH_6$ | $AH_3$-gel | $Al(OH)_3$ | $C_3ACcH_{11}$ |
|---|---|---|---|---|---|---|---|---|
| Schneider [7] | 1959 | DTA | ∼155 & ∼285 | | | | | |
| Ramachandran [8] | 1969 | DTA | ∼140–170 | ∼290 | | | | |
| Barnes and Baxter [9] | 1978 | DTG | ∼125 | | ∼330 | | ∼290 | |
| Day and Lewis [10] | 1979 | DTG | | | | 100–200 | 3 steps ∼550 | |
| Pope and Judd [11] | 1980 | DTA | ∼110–120 | | ∼320–350 | | ∼295–310 | |
| George [12] | 1983 | – | ∼140 | ∼170 | ∼300 | ∼90 | ∼280 | |
| Midgley [13] | 1984 | DTA | ∼150 | ∼230 | ∼310 | | ∼275 | ∼200 |
| Bushnell-Watson and Sharp [14] | 1985 | DTA | | ∼190–200 | | ∼107–120 | | 198 |
| Das et al. [15] | 1996 | DTA | ∼175 °C &160–180 | ∼275 & 200–280 | ∼320 | ∼300 | | |
| Guirado et al. [16] | 1998 | DTG | ∼(37, 99 & 112) | | | | | |
| Schmitt et al. [17] | 2000 | DTG | | | 200–400 | | | |
| Fryda et al. [18] | 2001 | DTA | ∼150 | ∼200 | ∼330 °C | | ∼290 | |
| Cardoso et al. [19] | 2004 | – | 120 | 170–195 | 240–370 | 100 | 210–300 | |

taneous differential thermal and thermo gravimetric analysis (DTA/TGA), $^{27}Al$ solid state NMR and temperature-dependent infrared spectroscopy (FT-IR) were also used.

The temperature-dependent infrared measurements were studied by two-dimensional infrared (2D-IR) correlation spectroscopy, a method that allows one to highlight various information which cannot be extracted easily from an ordinary one-dimensional spectrum. The experimental approach used in 2D-IR correlation spectroscopy is based on the detection of dynamic variations in the IR spectra of sample, obtained as a result of an external perturbation [29,30]. Since spectral peaks are spread over the second dimension in 2D-IR, the visualization of complex spectra consisting of many overlapped bands is simplified.

In the study the reported surface area evolution of thermally treated $C_2AH_8$ was measured by BET method.

## 2. Theoretical

Considerable variations occur in the position and relative intensity of the endothermic peaks in the reported DTA/DTG thermograms of $C_2AH_8$ preparations [24]. The water content of $C_2AH_8$ has been assigned to be 7–9 $H_2O$ molecules, but the fully hydrated compound is generally considered to contain 8 $H_2O$ molecules essential to the structure. In contrast to the $CAH_{10}$, several distinct lower hydrates with different XRD patterns are produced by dehydrating $C_2AH_8$ under various drying conditions. Uncertainty and controversy exists with regard to their composition and identity. According to Roberts [25], $C_2AH_{7.5}$, $C_2AH_5$ and $C_2AH_4$ are formed successively, as shown in Table 2. The 7.5 hydrate is obtained by drying at 34% relative humidity (r.h.), and the 5 hydrate at 12% r.h., or over anhydrous $CaCl_2$ or $P_2O_5$, or by heating at 102 °C. Composition of 5 hydrate was also evidenced in the high vacuum [30]. These two hydrates are very readily rehydrated to $C_2AH_8$ on exposure to air at 81% r.h., but the 4 hydrate, obtained by heating at 120 °C, does not rehydrate at this humidity. The constitution and bare existence of the alleged $C_2AH_4$ is uncertain.

The doubts concerning the exact structure of $C_2AH_8$ originate from the difficulty of preparing monocrystals of sufficient quality and preserving it from rapid dehydration and carbonation. The structure of $C_2AH_8$ was confirmed to be of the AFm (Al–Fe-mono) phases family of LDH compounds [20,21,31] which are structurally related to portlandite, $Ca(OH)_2$.

In cement chemistry the structure of AFm types of hydrates consists of cationic layers of $Ca_2Al(OH)_6^+$, separated by interlayers containing anions surrounded by water molecules. The OH anion (in $C_4AH_x$), or aluminate anion (in $C_2AH_{5–8}$) can be substituted by a wide range of other mono or di-valent anions, giving complex hydrates of the general formula: $[Ca_2Al(OH)_6]^+ [m/n\ X^{n-}\ (1-m)\ Al(OH)_4\ m\ Al(OH)_3\ y\ H_2O)]^-$, where $n$ is the valency of the substituting anion $X$ and $m$ is the degree of substitution. A solid solution between two end members, $C_4AH_x$ and $C_2AH_{5–8}$, occurs when, for example, $C_4AH_{19}$ absorbs aluminate ions from sodium aluminate solutions, without modification of the cation layers, as shown by XRD [32–34]. The $C_4AH_x$–$C_2AH_8$ solid solution range is given as lying between $m = 0.5$ and $m = 0.7$ [32].

Substitution of certain anions in the $C_2AH_8$ interlayers increase the stability to the structure, and reduces the rate at

Table 2
Physical properties of dicalcium aluminate hydrates [24,25]

| Compound | r.h./% | Crystal form | Density (g/cm$^3$) | Refractive indices | | Characteristic X-ray powder spacings (Å) |
|---|---|---|---|---|---|---|
| | | | | ω | ε | |
| $C_2AH_8$ | 81 | Hex. plates | 1.95 | 1.520 | 1.505 | 10.7, 5.36, 4.10, 3.96 |
| $C_2AH_{7.5}$ | 34 | Hex. plates | 1.98 | 1.520 | 1.505 | 10.6, 5.30, 3.53, 2.86 |
| $C_2AH_5$ | 12 | Hex. plates | 2.09 | 1.534 | 1.524 | 8.7, 4.34, 3.18, 2.87 |
| $C_2AH_4$[a] | (High vacuum) | Hex. plates | 2.27 | 1.565 | 1.559 | 7.4, 3.72, 2.87 |

[a] Exsistence doubtful.

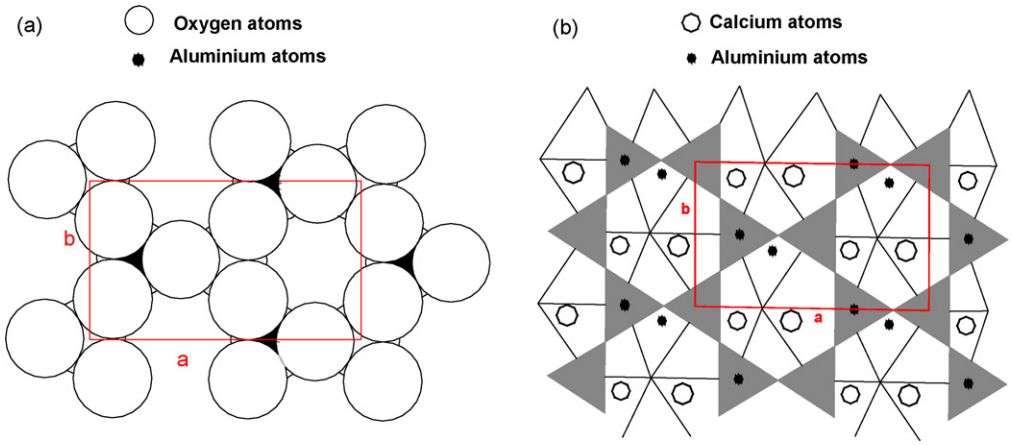


Fig. 1. Projection (001) of the structure of $C_2AH_8$. (a) Interlayer content (b) Stacking of tetrahedral interlayer above octahedral principal layer. Water molecules which raise the calcium coordination to seven (for clarity not presented) are located below and above the centers of a six-membered tetrahedral rings.

which conversion to $C_3AH_6$ occurs. The prevention of CAC hydrates conversion through formation of complex AFm-LDH hydrates has been investigated by Dosch et al. [34], Midgley [13] and Pérez [35,36].

Single crystal investigations on dicalcium aluminate hydrates [31] showed that the structures of di- and tetracalcium aluminate hydrates are closely related. The stacking of the layers in the 8 $H_2O$ hydrate is different from that in the 7.5 $H_2O$ hydrate. Both crystals are monoclinic. In the interlayer region only water molecules which raise the coordination of the Ca ions to seven could be located exactly. The remaining hydroxyl groups and water molecules are arranged in two levels of six-membered rings, the Al ions being distributed among the tetrahedral cavities, Fig. 1a. Because of low symmetry and random stacking of the principal layers a detailed crystal structure analysis was not possible. A refinement of the structure was possible from the $C_2AH_5$ crystal with trigonal space group R-3c, where each unit cell is composed of six double-layers lying perpendicular to *c*.

Based on the description of $C_2AH_8$ structure given by Scheller [31] and Richard at el. [20,21] as well as other analog LDH structures [37] in this paper we represent the structure of $C_2AH_8$ shown in Fig. 1. The structure of $[Ca_2Al(OH)_6]^+$ $[Al(OH)_4\ 3H_2O]^-$ consists of a principal layer derived from portlandite (CH) by the replacement of one third of $Ca^{2+}$ ions with $Al^{3+}$ ($Ca^{2+}$:$Al^{3+}$ = 2:1). In this positively charged layer, the heterovalent cations are distributed in such a way that each $Al^{3+}$ position is surrounded by six $Ca^{2+}$ positions, and each $Ca^{2+}$ site has three $Al^{3+}$ and three $Ca^{2+}$ sites as nearest neighbors. This layer then consists of $[Al(OH)_6]^{3-}$ octahedra distributed in an hexagonal primitive cell and connected by Ca atoms. The coordination of the Ca is increased to seven by water molecules in interlayer. Half of the aluminium atoms belong to the principal layer and are octahedrally coordinated. The other half is placed in the interlayer as $[Al(OH)_4]^-$ tetrahedrons. On the basis of the EXAFS and XRD analysis interlayer aluminium atoms were located at 5.35 Å from calcium [20]. Interlayer aluminium atoms occupy only half of the interlayer tetrahedral cavities (surrounded by hxdroxyl anions alone). The empty halves of the interlayer tetrahedral cavities are surrounded by three hydroxyl ions and one water molecule. The water molecules which rise Ca coordination number to seven fill the space below and above the centers of the six-membered rings (for the sake of clarity not shown on Fig. 1).

A monoclinic unit cell was proposed for $C_2AH_8$ structure [20] with the parameters: $a = 9.946$ Å, $b = 5.733$ Å, $c = 43.138$ Å and $\beta = 97.96°$. The cell side of the corresponding hexagonal principal layer is 5.740 Å.

Ambiguous data exist in the literature concerning the coordination of the interlayer aluminium. The $^{27}$Al NMR study of $C_2AH_8$ [22] indicated that the aluminium solely existed in octahedral coordination. On the other hand, Richard et al. [20,21] concluded by means of $^{27}$Al NMR and CP-MAS NMR that half the Al atoms in $C_2AH_8$ have octahedral, non-distorted coordination, whilst the other interlayer Al are in a strongly distorted tetrahedral coordinated site. The spectra were not published. XRD analysis indicated no impurities dedicated to anhydrous cement. Also, their IR study of $C_2AH_8$ was in agreement with the $^{27}$Al NMR.

Lastly, Faucon et al. [38] indeed observed tetrahedral coordinated Al in spectra but contributed it to a residual anhydrous aluminate impurity (with no XRD purity comments on prepared sample).

## 3. Experimental

### 3.1. Synthesis procedure

In the course of LDHs preparation with anions other than carbonate it is important to avoid contamination from $CO_2$, since the carbonate anion is readily incorporated and tenaciously held in the interlayer. Consequently, decarbonated and deionised water is used and exposure of the reacting material to the atmosphere is kept to a minimum.

Monocalcium aluminate (CA) and mayenite ($C_{12}A_7$) were synthesized and used for hydration reactions:

$$CA + C + 8H \rightarrow C_2AH_8 \quad (1)$$

$$C_{12}A_7 + 2C + 56H \rightarrow 7C_2AH_8 \quad (2)$$

For the syntheses of CA and $C_{12}A_7$, precipitated calcite ($CaCO_3$ analytical grade purity, Kemika) and gibbsite ($Al(OH)_3$, Sigma–Aldrich) have been wet homogenized in planetary mill (FRITSCH, Pulverisette 5, $\alpha$-Alumina pot and grinding balls) in the required stoichiometric mole proportion, dried at 105 °C and then fired at 1350 and 1300 °C, respectively, for 3 h in an air atmosphere electric furnace. $C_2AH_8$ was then prepared by shaking the mixture, of the corresponding calcium aluminate and freshly prepared calcium oxide, with excess decarbonated and deionised water (total water to solid ratio of 20), for 24 h in a tightly closed plastic vial at room temperature. The hydrate $C_2AH_8$ formed was filtered and dried by rinsing with acetone (2-propanone) under a flux of nitrogen (99.999% $N_2$, MESSER). Samples were stored in sealed plastic bags and held in a refrigerator at −5 °C. Before analyses samples were additionally dried at 50% r.h and 22 °C.

### 3.2. Methods of characterization

Simultaneous differential thermal and thermo gravimetric analysis (DTA/TGA) were performed with a NETZSCH STA 409 at a heating rate of 10 °C/min in $N_2$ flow of 30 $cm^3$/min using $\alpha$-$Al_2O_3$ as standard. Samples placed in platinum crucibles contained approximately 40 mg.

The powder X-ray diffraction combined with temperature treatment was adopted in the present study. Phillips diffractometer PW1830 with a Cu Kα radiation was used, the scan step was 0.02° with collection time of 1 s. Temperature treatments were accomplished by successive heating of same meticulously prepared sample in an air atmosphere electric furnace.

Temperature programed FTIR spectra of samples dispersed in KBr matrix were recorded at a resolution of 4 $cm^{-1}$ on an ABB Bomem MB102 spectrometer, equipped with CsI optics, DTGS detector, and a Specac 3000 Series high stability temperature controller with heating jacket. Measurements were performed under atmospheric pressure in air. The baseline subtraction was done with GRAMS/32 software (Galactic Industries Corp., Salem, NH), and the synchronous and asynchronous correlations was obtained by using a sub-program that was written for the setting of Matlab 6.5 (The MathWorks, Inc., Natick, MA) according to the discrete Hilbert transform as defined by Noda [39].

$^{27}Al$ NMR spectra were measured on a 600 MHz Varian Unity Inova spectrometer equipped with a 5 mm Doty CPMAS probe head. Spectra were recorded in samples rotating at the magic angle with a frequency of 10 kHz using a single-pulse excitation. The width of the excitation pulse was 2 μs (30° flip angle), the repetition delay was 0.4 s and the number of scans was 400. Spectra was referenced to 1 M $Al(NO_3)_3$.

The specific surface area, $S_w$, was determined using the multiple BET method (Micromeritics, Gemini) with nitrogen gas as the adsorbate.

## 4. Results

$C_2AH_8$ has been successfully synthesized by two routes, according to reactions (1) and (2). The obtained product was crystalline $C_2AH_8$. The hydration by route (2), with $C_{12}A_7$ as a precursor, produced $C_2AH_8$ with better crystallinity, and that material was used in research.

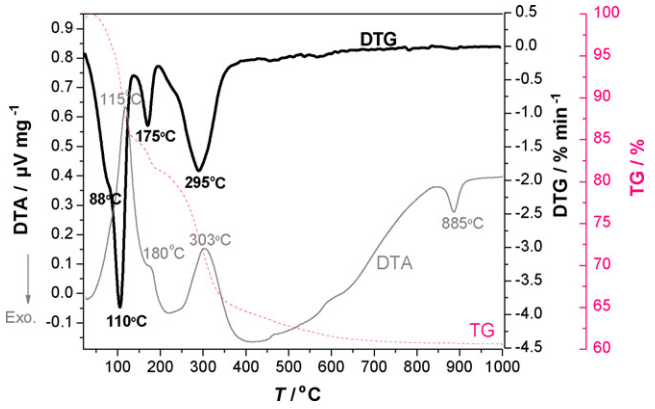


Fig. 2. DTA, TGA and derivative TGA traces of synthesized $C_2AH_8$ obtained with the heating rate of 10 °C $min^{-1}$.

Fig. 2 shows the result of the DTA/TGA analysis of the $C_2AH_8$ sample as a function of temperature. The TGA trace indicates three general regions of mass loss corresponding to three obvious dehydration peaks in the DTG curves. Thus, dehydration of $C_2AH_8$ is endothermic process which takes place in three main steps, at about 110, 175 and 300 °C, as shown in Fig. 2. It should be noted that DTA peaks occur about 5–8 °C later than the corresponding DTG peak, due to the thermal lag. The advantage of DTG curve over DTA curve is a straight baseline that allows quantification of the process taking place.

Results of XRD analysis indicated that pure $C_2AH_8$ (JCPDS file No. 11–205) with the good crystallinity have been obtained (Fig. 3 pattern at 25 °C). By increasing the temperature of the thermal treatment of the initial $C_2AH_8$ hydrate gives rise to the following products: $C_2AH_5$ and $C_2AH_4$, as shown in Fig. 3 by XRD patterns at 85 and 190 °C.

As the DTA analysis showed exothermic crystallizations at 885 °C (Fig. 2), samples of $C_2AH_8$ were heated in an air atmosphere electric furnace at the same rate as in the DTA/TGA

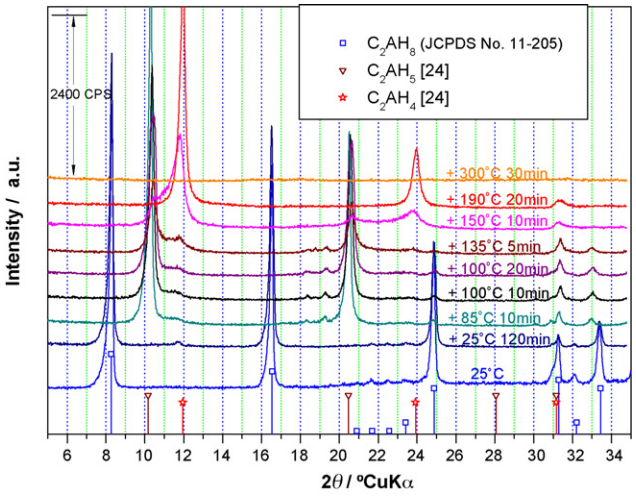


Fig. 3. X-ray diffraction patterns of $C_2AH_8$ synthesized and treated in the temperature range 25–300 °C.

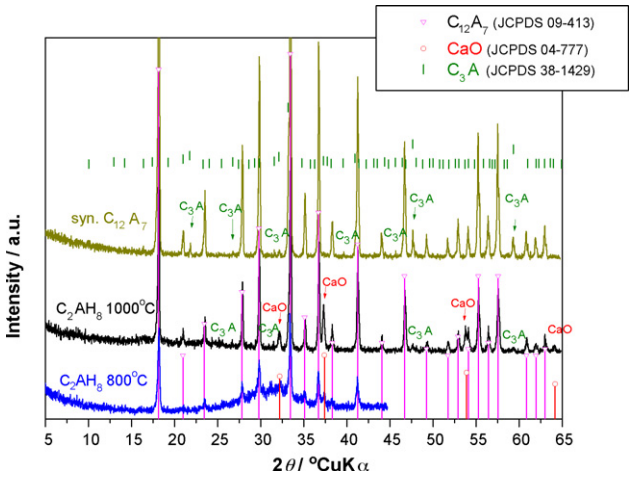


Fig. 4. X-ray diffraction patterns of synthesized $C_{12}A_7$ and $C_2AH_8$ fired at 800 and 1000 °C.

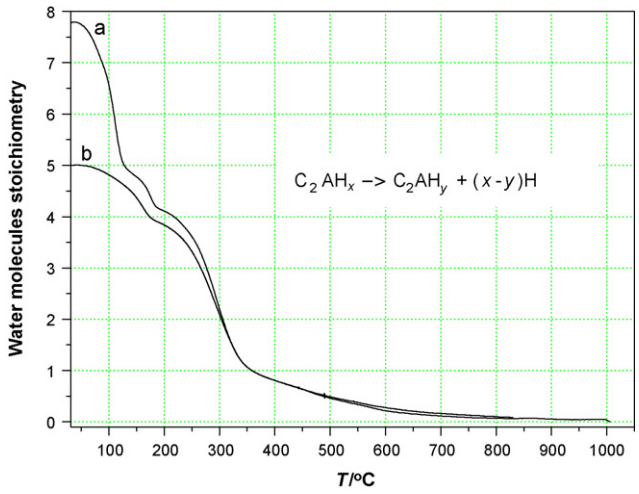


Fig. 5. Stoichiometry evolution of $C_2AH_y$ during thermal dehydration of the: (a) $C_2AH_8$ and (b) sample treated in the high vacuum (i.e. $C_2AH_5$).

experiment, up to the 800 and 1000 °C, and analyzed by XRD. The analysis showed (Fig. 4) that the main crystal phase formed is $C_{12}A_7$ with small quantities of CaO and $C_3A$. These analyses indicate the stoichiometry of $C_2A$ in the synthesized $C_2AH_8$.

The stoichiometry of the initial material studied is expressed as $C_2AH_x$, while the stoichiometry evolution as a function of temperature is expressed as $C_2AH_y$. The stoichiometry was calculated on the basis of the TGA results according to the following equations:

$$C_2AH_x \xrightarrow{T} C_2AH_y + (x - y)H \quad (4)$$

Initial composition of $C_2AH_x$ material studied is calculated (Eq. (5)) from the total weight loss of sample mass throughout the temperature range, up to 1000 °C, while stoichiometry at certain temperature, $y(T)$ is calculated from Eq. (6), taking into account current mass loss of the sample.

$$x = \frac{(1 - \mathrm{TG}_{T=1000\,^\circ\mathrm{C}})M_{C_2A}}{\mathrm{M}_H \mathrm{TG}_{T=1000\,^\circ\mathrm{C}}} \quad (5)$$

$$y(T) = \frac{M_{C_2A}}{M_H}(TG(T) - 1) + TG(T)x \quad (6)$$

$M_{C_2A}$ and $\mathrm{M_H}$ are molar masses of $C_2A$ and water respectively, and (1−TG) is relative mass loss of the sample based on the initial sample weight. Stoichiometry evolution of $C_2AH_y$ during thermal dehydration of the: (a) initial $C_2AH_8$ prepared and (b) the same material treated in the high vacuum is presented in Fig. 5. The stoichiometry of the initially prepared material is $C_2AH_{7.82}$, while after high vacuum treatment, the material composition is given by $C_2AH_5$.

Results of the thermal dehydration of the prepared $C_2AH_8$ studied by temperature-dependent FT-IR spectroscopy are shown in Figs. 6 and 7. For 2D-IR correlation analysis, spectra acquired at a heating rate of 1 K min$^{-1}$ in temperature range 30–250 °C (10 scans at a resolution of 4 cm$^{-1}$, acquisition time 30 s, recording time interval 90 s, temperature difference of 2 K between neighboring spectra) were processed. The 4000-400 cm$^{-1}$ spectral region was truncated by applying linear baseline at the end points. FTIR spectra were divided, according to the thermograms and XRD analysis, in two groups: (a) 30–110 °C and (b) 130–250 °C, and for each group the spectral data were subjected to mean normalization and centering as defined by Šašić et al. [40] prior the calculation of 2D-IR synchronous and asynchronous correlation spectra. It is worth noting that due to the lower heating rate in FT-IR experiment, there was enough time for decomposition processes to complete at lower temperatures.

Diagonal peak in a synchronous spectrum (autopeak) is always positive, and the magnitude of its intensity represents the overall extent of spectral intensity change, no matter whether the intensity is increasing or decreasing during the observed temperature interval. The peak located at the off-diagonal position (cross peak) can be positive or negative. A positive cross peak indicates that the peak intensities for the corresponding bands in the one dimensional (1D) spectrum are both increasing or both decreasing simultaneously, while a negative cross peak indicates that one peak intensity is increasing while the other is decreasing, or vice versa [29]. Since asynchronous spectra obtained gave no new insight regarding temperature dehydration of investigated samples they are not presented in this paper.

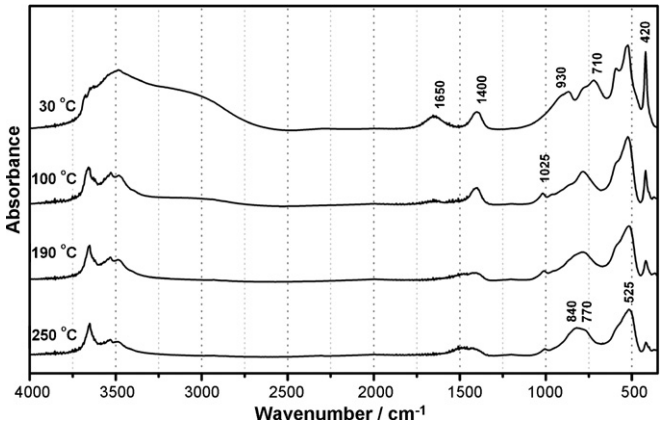


Fig. 6. FT-IR spectra of $C_2AH_8$ over a temperature range of 30–250 °C, heating rate 1 K/min.

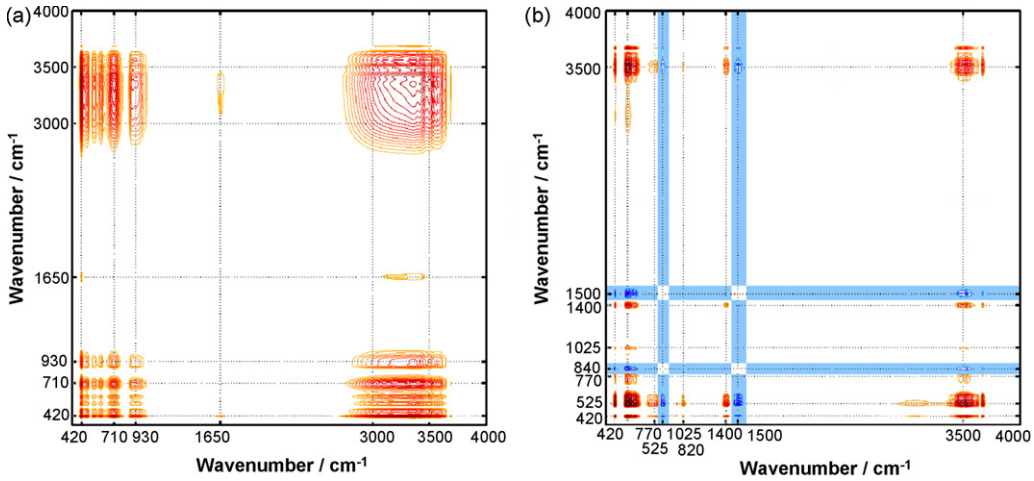


Fig. 7. Synchronous 2D-IR correlation spectrum of $C_2AH_8$ sample in the temperature interval (a) 30–110 °C and (b) 130–250 °C. Shaded (blue) areas indicate negative correlation intensity. (For interpretation of the references to color in this figure legend, the reader is referred to the web version of the article.)

The absorption band at 1400 $cm^{-1}$ in the FTIR spectrum of hydrate $C_2AH_y$ sample (Fig. 7) indicates a presence of interlayer $CO_3^{2-}$ impurities due to minor amounts of calcium aluminium hydroxide carbonate hydrate formed during FT-IR sample (pre)treatment (IR measurements were performed under atmospheric pressure in air). However, no traceable amount of the corresponding calcium aluminium hydroxide carbonate hydrate $[Ca_4Al_2(OH)_{12}]^{2+}$ $[CO_3\ 5H_2O]^{2-}$ (JCPDS file No. 87-0493) nor any other carboaluminates were evidenced by XRD, Fig. 4. In accordance with XRD results (Fig. 3) FT-IR showed no traceable amounts of either C, CA, $C_{12}A_7$ or $C_3A$ (Fig. 6).

The rehydration and carbonation was carried out on $C_2AH_4$ sample at 100% r.h. and 22 °C for 48 h. The powder XRD patterns for $C_2AH_4$ and the rehydrated sample are presented in Fig. 8.

The measurement of $C_2AH_8$ surface area by BET was impossible because of the high vacuum pretreatment. The measured surface areas of the thermally treated samples are: sample treated 10 min at 100 °C, $S_w(C_2AH_5) = 6.0\ m^2/g$; sample treated 30 min at 190 °C, $S_w(C_2AH_4) = 6.1\ m^2/g$; and sample treated 30 min at 300 °C, $S_w = 11.0\ m^2/g$.

## 5. Discussion

The $^{27}Al$ MAS NMR spectrum of the dicalcium aluminate hydrate, Fig. 9, consists of a sharp peak at 12 ppm and a broad peak between 40 and 80 ppm. $^{27}Al$ is a high sensitivity nucleus that yields broad lines over a wide chemical shift range. $^{27}Al$ is a spin 5/2 nucleus and is therefore quadrupolar. As a result, the signal width increases with asymmetry of the environment with somewhat broad lines in symmetrical environments but very broad lines in asymmetric ones.

The peak at 12 ppm was related to an octahedrally coordinated aluminium; the broad peak between 40 and 80 ppm indicated the presence of distorted $[Al(OH)_4]^-$ tetrahedral. This result differs from the spectrum previously reported by Gessner et al. [22] and Faucon et al. [38] but is in agreement with Richard et al. [20,21].

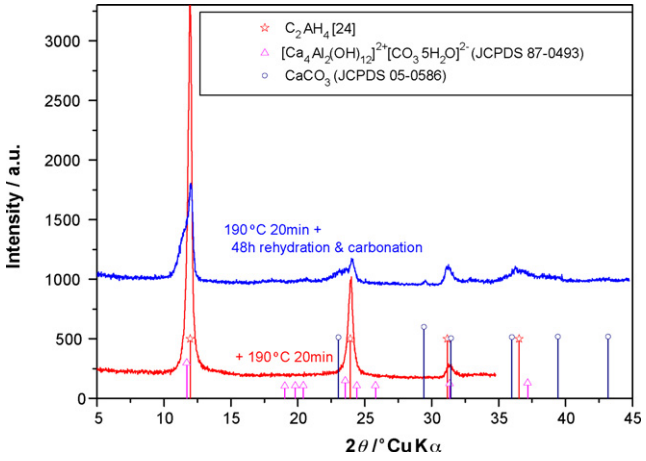


Fig. 8. The powder XRD patterns for $C_2AH_4$ and the rehydrated/carbonated sample treated at 100% r.h. and 22 °C for 48 h.

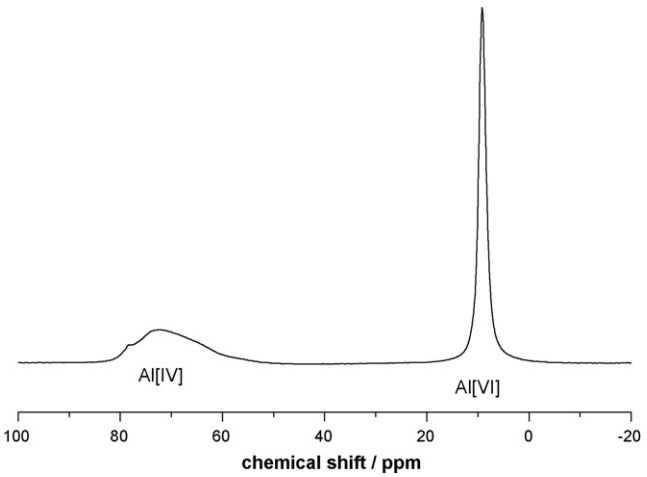


Fig. 9. $^{27}Al$ (165.252 MHz) MAS NMR spectra of $C_2AH_8$ sample.

Based on previous characterization of $AlO_4$ tetrahedra in CA, $C_{12}A_7$ and θ-$Al_2O_3$ and $AlO_6$ octahedra in calcium aluminate hydrates by Tarte [41], features related to the Al–O vibrations were located at 500–680 and 700–900 $cm^{-1}$, Fig. 6. The former absorption, common to all calcium aluminate hydrates spectra, is assigned to octahedrally coordinated aluminium. The latter absorption, manifested only in the $C_2AH_8$ hydrate IR spectrum, is assigned to tetrahedrally coordinated aluminium [41] in agreement with the $^{27}Al$ NMR results.

From the results obtained and proposed structure of $C_2AH_8$ shown in Fig. 1a variety of structural transformations observed are explained as a consequence of the removal of loosely held interlayer water molecules at lower temperatures, followed by grafting process of the interlayer $[Al(OH)_4]^-$ anion, as depicted in Fig. 10. Structural model of a grafting process of the interlayer $[Al(OH)_4]^-$ tetrahedron onto hydroxylated octahedrons of $[Ca_2Al(OH)_6]^+$ layers (Fig. 10c) has been proposed in order to explain observed loss of one water molecule, shrinkage of interlayer spacing and qualitative changes of FT-IR spectra.

The three events occurring in the course of thermal analysis, Fig. 2 can be well-explained using XRD data (Figs. 3 and 8). The XRD patterns (Fig. 3) exhibit the sharp characteristic diffraction lines appearing at $2\psi$ angle (8.26°, 16.54°, 24.87°); (10.17°, 20.46°, 31.16°) and (11.96°, 23.92°, 36.53°), respectively, which are ascribed to diffractions by planes (0 0 *l*), (0 0 2*l*) and (0 0 3*l*), corresponding to the basal spacing and its higher order diffractions. The shift of the basal spacing *d* from 10.7 to 8.7 Å and further to 7.4 Å may be explained by the shrinkage of layers due to the removal of physisorbed and interlayer water molecules (10.7 Å → 8.7 Å), and grafting process (8.7 Å → 7.4 Å). The XRD results at 135 and 150 °C, intermediate between first two processes, suggests that multiple crystalline phases in the treated sample coexist.

Structural studies of LDHs show that interlayer anions are positioned to have their oxygens (OH-groups) forming hydrogen bonds with hydrogens of the OH-groups of the adjacent octahedral (principal) layers [37] or vice versa. In this way the position and orientation of the interlayer anions determine the layer stacking and its periodicity along *c* axis. It means that the hydroxyls of the $[Al(OH)_4]^-$ tetrahedrons are located along the *c* axis near the OH groups of the neighboring octahedral (principal) layers and forms hydrogen bonds responsible for layer interaction in samples thermally treated between 85–190 °C, Fig. 10b and c.

Short basal spacings of 7.4 Å for samples treated at 150 °C and higher are incompatible with the presence of "free" $[Al(OH)_4]^-$ anions. The only consistent hypothesis is the grafting [37] of the anions onto the LDH layers with elimination of water, leading to neutral layers. The new phase has to be considered as a layered oxy-hydroxy-salt and belongs no more to the LDHs family. The structure of the $C_2AH_4$ interlamellar domains is described as an ordered arrangement of interlayer $[Al(OH)_4]^-$ tetrahedral, retaining their $C_3$ symmetry axis perpendicular to the layer, with one oxygen shared with a principal octahedral layer and the three other OH facing three OH groups of the opposite layer by forming hydrogen bonds, Fig. 10c. This condensation is rendered possible by compatible hexagonal symmetry (Fig. 1) of the two layers (tetrahedral and octahedral) which possess condensable OH groups.

Therefore, first dehydration peak in Fig. 2 occurring approximately at 110 °C is due to a desorption of physisorbed and interlayer water molecules. The second dehydration peak, occurring at 175 °C corresponds to the grafting process of the interlayer anions. The third broad dehydration peak is a consequence of a dehydroxylation of the lattices and decomposition of the interlayer anions. Dehydroxilation of OH bound to tetrahedral Al is claimed as the origin of a stage 200–240 °C, while the stage 240–330 °C has been attributed to dehydroxilation of OH octahedraly bound to Ca and Al. It can be argued that octahedral Al–OH decomposes after the interlayer tetrahedral Al–OH due to greater compactness of octahedral layer. The assumption is corroborated with the fact that within the third dehydration DTG peak a small shoulder (fewer tetrahedral OH groups) on the left side is observed followed with the majority of the third dehydration peak.

According to the TGA results the stoichiometry of the water loss (Fig. 5) is explained as follows: three interlayer water molecules are lost during first dehydration peak at about 110 °C, one water molecule is eliminated by the grafting of the tetrahedral anions onto the octahedral layers during second peak at about 175 °C, and four molecules of water exit structure during third dehydration peak, which is in agreement with the structural model given in Figs. 1 and 9.

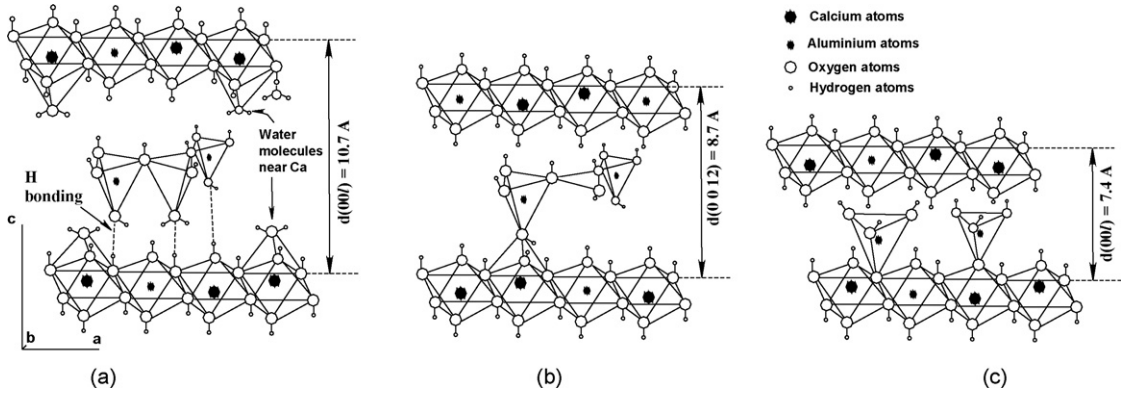


Fig. 10. Structural transformations of a $C_2AH_y$ related to the dehydration process. Schematic diagrams of structural arrangement of: (a) $C_2AH_8$, (b) $C_2AH_5$, and (c) $C_2AH_4$.

On heating at 300 °C or above, all (0 0 *l*) diffraction lines of XRD pattern vanish (Fig. 3) due to the complete decomposition of the interlayer anions, and thus the XRD pattern present an amorphous dehydration product until the $C_{12}A_7$, CaO and $C_3A$ crystallizations at 800 and 1000 °C (Fig. 4).

The further confirmation of the presence of the grafting process is both the hindered rehydration and anion exchange with carbonate anions for the $C_2AH_4$ sample. The rehydration and carbonation was carried out on $C_2AH_4$ sample treated at 100% r.h. and 22 °C for 48 h in an air atmosphere. The powder XRD patterns for $C_2AH_4$ and the rehydrated sample are presented in Fig. 8. It is seen that after anion exchange with carbonate the positions of the characteristic diffractions lines are almost the same as those before carbonation with only minor traces of the characteristic diffractions for $[Ca_4Al_2(OH)_{12}]^{2+}$ $[CO_3\ 5H_2O]^{2-}$ (JCPDS No. 87-0493) and calcite ($CaCO_3$), due to slow carbonation. The result suggests the $C_2AH_4$ rehydration has been hindered due to the grafted $[Al(OH)_4]^-$ anions, although water and carbonate has a large affinity for LDHs containing Ca and Al. Contrary to $C_2AH_4$ the $C_2AH_5$ hydrate is very readily rehydrated to $C_2AH_8$ and very readily carbonates on exposure to air at 81% r.h [24,25].

In the synchronous spectrum (Fig. 7a) obtained for 30–110 °C temperature interval one can depict strong autopeaks, associated with removal of intrinsic water molecules in the interlayer region, at 3400–3000 (OH stretching vibrations), 1650 (HOH-bending), 930, 710 and 420 $cm^{-1}$ (low-frequency rotational modes of $H_2O$). Water HOH bending mode at 1650 $cm^{-1}$ directly represents the amount of water molecules in the sample. In general the strong and broad band observed around 3400–3000 $cm^{-1}$ corresponds to the OH stretching vibration of surface and interlayer water molecules, which are found at lower frequency in LDHs compared with the OH stretching vibration in free water at 3600 $cm^{-1}$. This broad band is related to the formation of hydrogen bonding of interlayer water with the interlayer anions as well as with hydroxide groups of layers [37].

Additional heating of $C_2AH_8$ creates significant perturbation in the principal layer, as can be seen from the synchronous spectrum (Fig. 7b) obtained for 130–250 °C temperature region. The HOH-bending mode of the interlayer water around 1650 $cm^{-1}$ has disappeared as well as the broad band related to the formation of hydrogen bonding of interlayer water, while in the OH stretching region bands associated with the hydroxide sheets are observed at >3400 $cm^{-1}$. During heating the M–O stretching modes, hidden in the broad band 3400–3700 $cm^{-1}$, are observed to shift toward higher frequencies while decreasing in intensity. The autopeaks at 1025, 770 and 525 $cm^{-1}$ were assigned to the stretching and bending vibrations of the Al–O bonds. The change in bands observed in the low-frequency region of the spectrum <1100 $cm^{-1}$ attributed to Me–OH vibrations indicates the reconstruction of the structure.

The autopeaks at 1500 and 840 $cm^{-1}$ are associated with only two bands that are ascending (Fig. 7b), as depicted by negative cross peaks with the rest of the spectrum. Their origin could be attributed to a proposed grafting process and formation of carbonate impurities by reaction with atmospheric $CO_2$.

The surface area increases during thermal treatment of samples, probably because of the formation of channels and chimneys through the octahedral layers [42] due to $H_2O$ vapor evolution during thermal decomposition, which is consistent with the amorphisation of the starting material in the third dehydration process.

## 6. Conclusion

$C_2AH_8$ has been successfully synthesized by two routes, and obtained product was predominately crystalline. As seen from the results of thermal analysis, dehydration of $C_2AH_8$ proceeds in three main steps, during which a loss of three (at 110 °C), one (at 170 °C) and four molecules of water (at 300 °C) occurs. In those three main steps the following processes take place: desorption of physisorbed and interlayer water, grafting of interlayer anions onto the principal layer, dehydroxylation of the lattice and decomposition of interlayer anions. The processes are also evidenced by XRD because they lead to variety of structural transformations. The lowest basal spacing of distinct hydrate obtained by $C_2AH_8$ thermal dehydration ($C_2AH_4$) arises from grafting reaction (8.7–7.4 Å transformation) of anionic tetrahedron of interlayer $[Al(OH)_4]^-$ with hydroxyl groups on the octahedral principal layers of the host structure. At the highest temperatures studied (800 and 1000 °C), the amorphous material formed during the dehydration and collapse of the structure at 300 °C, crystallizes again giving mainly $C_{12}A_7$ with small quantities of $C_3A$ and CaO as final products. The results provide better insight in $C_2AH_8$ thermal evolution but due to a DTG peaks overlapping, quantitative analysis of CAC hydration products is still difficult. Toward a rational (qualitative and quantitative) interpretation by thermal analysis more work is needed in order to correlate the thermal behavior of pure hydration products and real mixes of CAC hydration products. Furthermore, one has to bear in mind that the composition of hydrated material depends on the conditions of storage, thus complicating thermal analysis. From the results obtained, it is incorrect to ignore the contribution of $C_2AH_8$ to the total mass loss during thermal analysis of CAC hydration products in the low temperature range (less than 170 °C).

## Acknowledgements

The authors acknowledge financial support from the Croatian Ministry of Science Education and Sports under project's no. 125-1252970-2983 and no. 098-0982904-2927. Dr G. Mali is gratefully acknowledged for his contribution in $^{27}Al$ NMR measurement.

## References

[1] R.J. Mangabhai (Ed.), Calcium Aluminate Cements, Chapman and Hall, London, 1990, pp. 39–241.
[2] R.J. Mangabhai, F.P. Glasser (Eds.), Calcium Aluminate Cements 2001, IOM Communications, London, 2001, pp. 151–246.
[3] J. Bensted, High alumina cement-Present state of knowledge, Zement-Kalk-Gips 46 (1993) 560–566.

[4] T. Matusinovic, N. Vrbos, D. Curlin, Lithium salts in rapid setting high-alumina cement materials, Ind. Eng. Chem. Res. 33 (1994) 2795–2800.
[5] T. Matusinovic, N. Vrbos, J. Sipusic, Rapid setting and hardening calcium aluminate cement materials, Zement-Kalk-Gips International 5 (2005) 72–79.
[6] K.L. Scrivener, J.L. Cabiron, R. Letourneux, High-performance concretes from calcium aluminate cements, Cem. Concr. Res. 29 (1999) 1215–1223.
[7] S.J. Schneider, Effect of Heat-Treatment in the Constitution and Mechanical Properties of Some Hydrated Aluminous Cements, J. Amer. Ceram. Soc. 42 (1959) 184–193.
[8] V.S. Ramachandran, Applications of Differential Thermal Analysis in Cement Chemistry, Chemical Publishing Company, New York, 1969, pp. 206–212 (Chapter VIII.2).
[9] P.A. Barnes, J.H. Baxter, A critical analysis of the application of derivative thermogravimetry to the determination of the degree of conversion of HAC, Thermochim. Acta 24 (1978) 427–431.
[10] D.E. Day, G. Lewis, Quantitative thermogravimetry of calcium aluminate compounds and cements after hydrothermal treatment, Bull. Am. Ceram. Soc. 58 (1979) 441–444.
[11] M.I. Pope, M.D. Judd, Differential Thermal Analysis, Heyden & Son, London, 1980, pp. 147–155.
[12] C.M. George, Industrial alumina cement, in: P. Barnes (Ed.), Structure and Performance of Cement, 1983.
[13] H.G. Midgley, Measurement of high-alumina cement-calcium carbonate reactions using DTA, Clay Miner. 19 (1984) 857–864.
[14] S.M. Bushnell-Watson, J.H. Sharp, The detection of the carboaluminate phase in hydrated high alumina cements by differential thermal analysis, Thermocim. Acta 93 (1985) 613–616.
[15] S.K. Das, A. Mitra, P.K. Dad Padar, Thermal analysis of hydrated calcium aluminates, J. Therm. Anal. 47 (1996) 765–774.
[16] F. Guirado, S. Gali, J.S. Chinchon, Thermal dehydration of $CAH_{10}$, Cem. Concr. Res. 28 (1998) 381–390.
[17] N. Schmitt, J.F. Hernandez, V. Lamour, Y. Berthaud, P. Meunier, J. Poirier, Coupling between kinetics and dehydration, physical and mehanical behaviour of high alumina castable, Cem. Concr. Res. 30 (2000) 1597–1607.
[18] H. Fryda, K.L. Scrivener, G. Chanvillard, Relevance of laboratory tests to field applications of calcium aluminate cement concretes, in: R.J. Mangabhai, F.P. Glasser (Eds.), Calcium Aluminate Cements 2001, IOM Communications, London, 2001, pp. 227–246.
[19] F.A. Cardoso, D.M.M. Innocentini, M.M. Akiyoshi, V.C. Pandolfelli, Effect of curing time on the properties of CAC bonded refractory castables, J. Eur. Ceram. Soc. 24 (2004) 2073–2078.
[20] N. Richard, N. Lequeux, P. Boch, Local environment of Al and Ca in $CAH_{10}$ and $C_2AH_8$ by X-ray absorption spectroscopy, Eur. J. Solid State Inorg. Chem. 32 (1995) 649–662.
[21] N. Richard, N. Lequeux, P. Boch, EXAFS study of refractory cement phases: $CaAl_2O_{14}H_{20}$, $Ca_2Al_2O_{13}H_{16}$, and $Ca_3Al_2O_{12}H_{12}$, J. Phys. III France 5 (1995) 1849–1864.
[22] W. Gessner, D. Müller, H.-J. Behrens, G. Scheler, Zur Koordination des Aluminiums in den Calciumaluminathydraten $2CaO{\cdot}Al_2O_3{\cdot}8H_2O$ und $CaO{\cdot}Al_2O_3{\cdot}10H_2O$, Z. anorg. allg. Chem. 486 (1982) 193–199.
[23] N. Richard, N. Lequeux, P. Florian, Changes in structure of $CaAl_2O_{14}H_{20}$ during heat treatments: X-ray absorption spectroscopy and 27Al NMR studies, in: P. Colombet, A.-R. Grimmer, H. Zanni, P. Sozzani (Eds.), Nuclear Magnetic Resonance Spectroscopy of Cement-Based Materials, Springer, Berlin, 1998, pp. 321–329.
[24] F.M. Lea, The Chemistry of Cement and Concrete, third ed., Edward Arnold, London, 1970, pp. 204–235.
[25] M.H. Roberts, New calcium aluminate hydrates, J. Appl. Chem. 7 (1957) 546–5443.
[26] T.R. Jensen, A.N. Christensen, J.C. Hanson, Hydrothermal transformation of the calcium aluminum oxide hydrates $CaAl_2O_4{\cdot}10H_2O$ and $Ca_2Al_2O_5{\cdot}8H_2O$ to $Ca_3Al_2(OH)_{12}$ investigated by in situ synchrotron X-ray powder diffraction, Cem. Concr. Res. 35 (2005) 2300–2309.
[27] S. Rashid, X. Turrillas, Hydration kinetics of $CaA1_2O_4$ using synchrotron energy-dispersive diffraction, Thermochim. Acta 302 (1997) 25–34.
[28] K.L. Scrivener, H.F.W. Taylor, Microstructural development in pastes of a calcium aluminate cement, in: R.J. Mangabhai (Ed.), Calcium Aluminate Cements, Chapman and Hall, London, 1990, pp. 41–51.
[29] Y. Ozaki, I. Noda, Two-Dimensional Correlation Spectroscopy, Wiley, Chichester, 2004.
[30] I. Noda, Generalized two-dimensional correlation method applicable to infrared, Raman, and other types of spectroscopy, Appl. Spectrosc. 47 (1993) 1329–1336.
[31] Th. Scheller, H. J. Kuzel, Studies on dicalcium aluminate hydrates, The 6th International Congress on the Chemistry of Cement, Moscow, 1974, Section II, Suppl. Paper.
[32] W. Dosch, H. Keller, On the crystal chemistry of tetracalcium aluminate hydrate, The 6th International Congress on the Chemistry of Cement, Moscow, 1974, Section III, Suppl. Paper.
[33] W. Dosch, H. Keller, H. zur Strassen, Additional remark on tetracalcium aluminate hydrate and its quaternary complex salts, Proceedings of the 5th International Symposium on the Chemistry of Cement, Tokyo, 1968, Written Discussion No. II-21, 72-77.
[34] W. Dosch, C. Koestel, Stabilized dicalcium aluminate hydrates, US Patent 4095989, 20 June, 1987.
[35] M. Pérez, T. Vázquez, F. Triviño, Study of stabilized phases in high alumina cement mortars, Part II. Effect of $CaCO_3$ added to high alumina cement mortar subjected to elevated temperature curing and carbonation, Cem. Concr. Res. 14 (1984) 1–10.
[36] M. Pérez, T. Vázquez, F. Triviño, Study of stabilized phases in high alumina cement mortars, Part I. Hydration at elevated temperatures folowed by carbonation, Cem. Concr. Res. 13 (1983) 759–770.
[37] V. Rives (Ed.), Layered Double Hydroxides: Present and Future, Nova Science Publishers, New York, 2001, pp. 18–139.
[38] P. Faucon, T. Charpentier, D. Bertrandie, A. Nonat, J. Virlet, J.C. Petit, Characterization of calcium aluminate hydrates and related hydrates of cement pastes by $^{27}$Al MQ-MAS NMR, Inorg. Chem. 37 (1998) 3726–3733.
[39] I. Noda, Determination of Two-Dimensional Correlation Spectra Using the Hilbert Transform, Appl. Spectrosc. 54 (2000) 994–999.
[40] S. Šašić, A. Muszynski, Y. Ozaki, A new possibility of the generalized two-dimensional correlation spectroscopy. 2. Sample-sample and wavenumber-wavenumber correlations of temperature-dependent near-infrared spectra of oleic acid in the pure liquid state, J. Phys. Chem. 104 (2000) 6388–6394.
[41] P. Tarte, Infra-red spectra of inorganic aluminates and characteristic vibrational frequencies of $AlO_4$ tetrahedra and $AlO_6$ octahedra, Spectroch. Acta 23A (1967) 2127–2143.
[42] W.T. Reichle, S.Y. Kang, D.S. Everhardt, The nature of the thermal decomposition of a catalytically active anionic clay mineral, J. Catal. 101 (1986) 352–359.